Energy Proceedings
Vol 26, 2022
ISSN 2004-2965

# Open Centre Turbines: From the Wake Analysis to The Array Design#

Giacomo Lo Zupone[1], Changjun Liu [2], Jinyue Yan[3], Bin Liang[1*]

1 Institute of New Energy and Low-carbon Technology, Sichuan University, 610207 Chengdu, PRC

2 School of Chemical Engineering, Sichuan University, Chengdu 610065, PRC

3 The Royal Institute of Technology (KTH), Division of Energy Processes, Stockholm, Sweden

**ABSTRACT**

The open centre turbine can be easily installed with a kite-like mooring system. It is promising to harvest the renewable marine resources due to its higher energy conversion efficiency, lower cost, and minimum impacts on the submarine environment. However, multi-devices deployment is still a great challenge due to the interaction between the mutual wakes.

This work deals with the wake morphology and the multi-device configuration by applying the Computational Fluid Dynamic analysis. A fully resolved model reveals that most of the turbulence affects the wake within 2D axial distance (twice the turbine diameter), with a maximum radial amplitude of 1.6R. In the axial direction, after 2D, due to an induced "suction effect" by the annular geometry, the wake takes a cylindrical shape.

For a 2 turbines array, a wheelbase of 2.5D and an interplane of 5D allow keeping the devices' performances constant.

**Keywords:** open centre turbine, wake phenomena, tidal, multi-device farm, tidal turbine farm

**NOMENCLATURE**

| *Abbreviations* | |
|---|---|
| $R$ | Rotor radius |
| $D$ | Rotor diameter [m] |
| $A_0$ | Turbine rotor area [m$^2$] |
| $v$ | Flow velocity [m/s] |
| $v_o$ | Undisturbed flow velocity [m/s] |
| $C_T$ | Thrust coefficient [-] |
| $C_p$ | Power coefficient [-] |
| $T$ | Thrust [N] |
| $M$ | Turbine torque [Nm] |
| $a$ | Axial induction factor [-] |
| $a'$ | Tangential induction factor |
| $m$ | Wheelbase between turbines |
| $b$ | Number of blades [-] |
| $p$ | Static pressure [Pa] |
| $k$ | Wake aperture coefficient |
| $\alpha$ | Blade attack angle |
| $\gamma$ | Blade pitching angle |
| $\varphi$ | Blade inflow angle |
| $\vartheta$ | Axial velocity deficit [-] |
| $\lambda$ | Tip speed ratio [-] |
| $\rho$ | Water density [kg/m$^3$] |
| $\omega$ | Turbine angular velocity [rad/s] |

## 1. INTRODUCTION

Tidal kinetic turbines have been capturing the attention of the researchers and engineers, although, the yielded energy, depending on the rotor swept area, is moving the focus on the farm concept. The farm approach is more suitable to harvest the maximum power from a given site, taking advantage from lower costs of installation due to the sharing of the transmission cables and devices components. For an efficient farm design, it is of paramount importance the study of the wake phenomena induced by the devices.

An initial numerical approach, adopting the wind turbine design framework, was deployed by Jensen [1] (1983) and Larsen [2] (1988). However, Bahaj et al [3] (2007) conducted some studies characterizing the wake phenomena on tidal turbines. The main performance calculations have been suggested by Chen [4] (2017), approaching the nesting strategy. Some experimental data have been recently reported by Zhang et al [5] (2017).

Stansby and Stallard [6] (2016) conducted a deeper investigation on wake phenomena for array layouts using Computational Fluid Dynamic (CFD) analysis.

The research was then developed by Ahmadi et al [7] (2019), indicating the acceptable turbine axial distance as 7 diameters and the radial one 3. Recently, some experiments have been conducted by Badoe et al [8] (2022), testing 3 scaled models in a facility, and then correlating data and CFD investigation.

In this panorama, the open centre concept, subject of this paper, born in 2010, has been conceived to fulfil

some tidal turbines' gaps. The traditional devices are dramatically affected by high Capital and Operational expenditures due to the huge installation structures, whose basements are moored on the seabed, involving complex underwater works.

An early study was developed by Barbarelli et al [9] (2013), describing a full floating turbine moored to the coast like a kite: it was controlled by the aerodynamic laws under simply equilibrium equations.

The first open centre turbine manufacturing and installation costs were assessed by Lo Zupone et al [10] (2016), by calculating the cost of produced energy. It amounts to 0.134 €/kWh for a pilot turbine of 12 m diameter. Barbarelli et al [11] (2018) demonstrated the cost-effectiveness of this technology, by replacing a 12 m diameter turbine with 5 smaller ones (5 m diameter) at the same energy output.

Lo Zupone et al [12] (2020) addressed some further technical gaps. They introduced a mooring line made by heavy and light nodes connected by tubular elements, where all the positioning add-ins (wings and floaters) are installed over the mooring fixture.

The last gap is the wake morphology, to select the axial and radial clearances between turbines for a future array design. Due to the novelty of this design concept [13] (2022), the author initially investigates the turbine wake phenomena, by carrying out a CFD analysis.

## 2. METHODS

### *2.1 Wake morphology: Jensen model*

According to the Jensen model [14], widely used for this purpose, a few assumptions must be introduced for the initial study.

- A single turbine is considered.
- No effects of the seabed and sea surface.
- No boundary layer interaction.

Referring to Figure 1, and assuming a coordinate frame with the origin in the turbine centre, the wake develops following [15] the eq. (1):

$$y = y_0 + kz \tag{1}$$

where $y_0 = R$ is the turbine radius, $y$ is the radial distance, $z$ is the distance from the rotating plane, and $k$, also defined "decay" in [16], is the wake conicity ($\delta$ is the cone aperture angle).

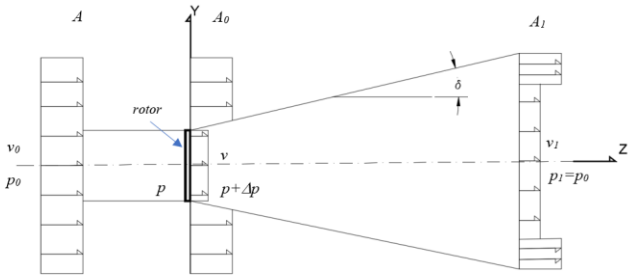


*Figure 1: flow near a turbine rotor: pressure and velocity, reference sections and wake parameters*

The velocity field behind the turbine can be evaluated starting from the momentum balance equation [17]:

$$\pi r_0^2 v + \pi v_0 (y^2 - y_0^2) = \pi r^2 v \tag{2}$$

By introducing $C_T$, the thrust coefficient, it can be written:

$$\frac{v}{v_0} = 1 - 2a = \sqrt{1 - C_T} \tag{3}$$

where $a$ is the axial induction factor. By merging the eq. (1), (2) and (3), the velocity behind the turbine is obtained [181] as:

$$v = v_0 + v_0 (\sqrt{1 - C_T} - 1) \left(\frac{y_0}{y}\right)^2 \tag{4}$$

The CFD analysis will provide, at every fixed $z$, the flow axial velocity, so to accommodate the wake morphology and, in addition, trough the eq. (4), to arrange an analytical model.

### *2.2 CFD approach*

As mentioned in the introduction, the paper aims to analyse the flow field using the Computational Fluid Dynamic (CFD) [19].

In the current study the RANS equations, mass and momentum conservation, must be solved for an incompressible flow [20]. The Reynolds stress term requires a turbulence model to close the equations, so the *k-ω SST* (Shear Stress Transport) has been selected [21]. The CFD analysis was conducted with ANSYS Fluent commercial CFD code (version 19.0 R3).

### *2.3 CAD model*

The turbine is composed as in Figure 2, in the single rotor configuration, by a toroidal stator (1) where a bladed rotor (2) slides reducing the friction thanks to a ball bearing (6). The kinetic energy is converted in electricity by a permanent magnet generator. Its rotating part (4), with the installed magnets (5), is housed into the blade rotor and the static one (3), whereas the coils (not visible), in the turbine stator.

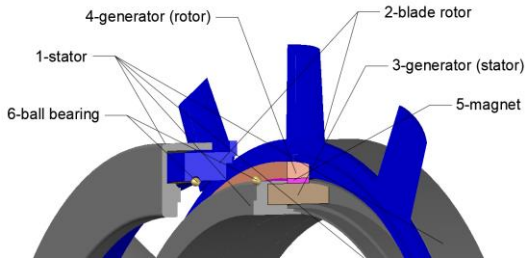


*Figure 2 main turbine components [13]*

The selected turbine parameters are listed in Table 1, and relate to the optimal design [10] for the maximum power output at a certain flow velocity and Tip Speed Ratio (TSR).

*Table 1 Turbine main parameters*

| Parameter | Symbol | Value |
|---|---|---|
| Blade profile | NACA 4 digits | 4412 |
| External diameter | D [m] | 1.12 |
| Central hole diameter | $D_i$ [m] | 0.96 |
| Tip Speed Ratio | λ [-] | 2.50 |
| Number of blades | b [-] | 12 |
| Rotor swept area | $A_0$ [$m^2$] | 0.26 |
| Rotational velocity | $\omega_0$ [rad/s] | 13.39 |
| Inflow angle | ϕ [rad] | 0.275 |
| Free stream velocity | $v_0$ [m/s] | 3.0 |
| Number of nodes (CFD model) | [-] | 930,949 |
| Number of elements (CFD model) | [-] | 4,414,026 |

### *2.4 Domain dimensions*

To capture the fluid field behind the turbine, according to [22], the inflow distance 3D, the inlet diameter 4D, and the streamwise distance 7D, have been selected. The early CFD runs confirmed that the axial velocity is recovered after 6D.

In the current investigation, due to the novelty of the study, a blockage ratio, $b_r$ = 0.012 (1.12%) has been selected, far from 5% indicated in [23] as limit without corrections.

### *2.5 CFD model and solver assessment*

To model the flow fields and the turbine rotating motion, the Moving Reference Frame (MRF) [24] has been adopted, for a steady analysis involving performances and flow field characterization. Based on the parameters resumed in Table 1, the turbine performances have been evaluated, to assess the solver and establish the grid independence. Table 2 resumes the main significant CFD output.

*Table 2: main CFD output data*

| Variable | Symbol | Output |
|---|---|---|
| Torque | *M* [Nm] | 111.47 |
| Power Coefficient | $C_p$ [-] | 0.485 |
| Thrust | *T* [N] | 1383.02 |
| Turbine Power | $P_t$ [W] | 1492.58 |

## 3. RESULTS

### *3.1 YZ plane analysis*

The previous results are more evident by introducing the axial velocity deficit as:

$$\vartheta = 1 - \frac{v}{v_0} \tag{5}$$

By introducing the CFD values into the eq. (5), the resulting curve is displayed in Figure 3. The trend highlights the flow alteration immediately behind the rotor as main peculiarity: the negative deficit indicates that the flow velocity is higher than the undisturbed one ($v_0$). It's such a Venturi effect, where the annular rotor represents the restricted section.

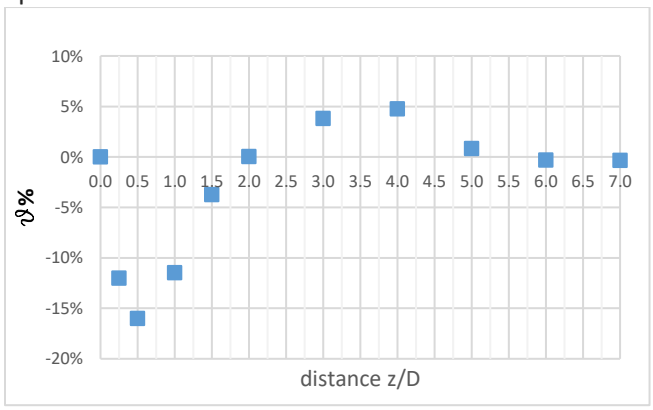


*Figure 3: Axial velocity deficit from CFD analysis*

To determine the full flow field characteristics, the investigation must be extended in the radial direction, into the XY-plane.

### *3.2 XY plane flow deployment*

To accommodate fully investigate the model, assuming *y/R* as radial distance from the rotor axis, the fluid domain is divided into 4 symmetrical zones, as depicted in Figure 4, and the axial velocities, at every *y/R,* are acquired from CFD.

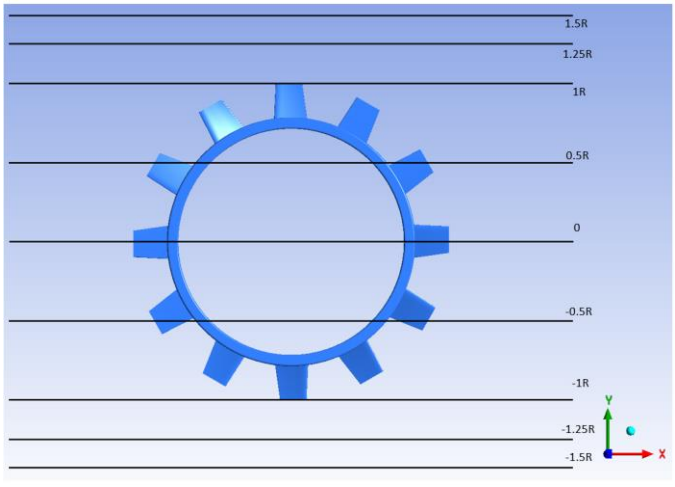


*Figure 4: front view flow field levels (not to scale)*

Figure 5 reports the axial velocity trend at every datum *y/R*, highlighting that, after 6D, the flow achieves $v_0$ (recovery condition) at any distance. It is noticeable that at 1R (grey curve), before 2D, the main effect of the blade downwash is affecting the flow. Whereas the 0.5R (orange) curve highlights the Venturi effect close to 0.5D, where the restricted section, due to the annulus (central hole), deploys its maximum effect. So, the investigation can be focused only within 2D axial distance.

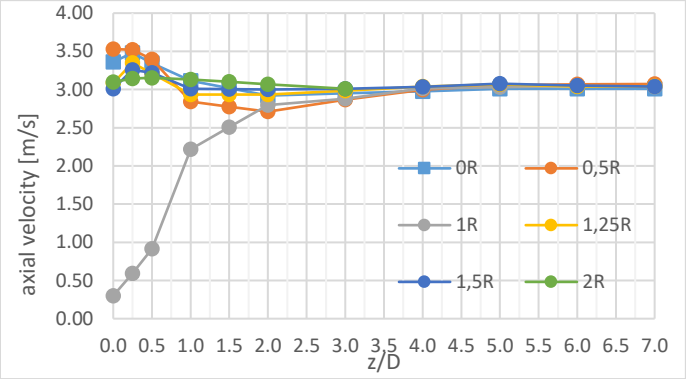


*Figure 5 axial velocity trends vs z/D*

In the range 0D ~ 2D (Figure 5), the maximum deficit is located near the rotor plane, at the ideal restricted section. The first evidence is that over 1.5R the axial velocity deficit is close to 1%, involving a slight flow field alteration at any axial distances.

Below 1.5R the flow field is characterized by 3 zones, as depicted in Figure 6: in the first one (*zone 1*), between 1.5R and 1R, the velocity deficit increases in the range 0.25D ~ 0.5D approaching the blade tip due to the induced tip vortices.

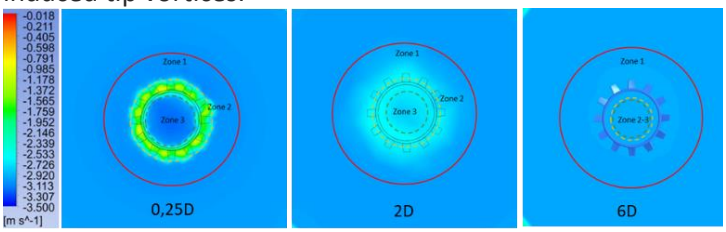


*Figure 6: flow field subdivision in 3 zone*

Into the *zone 2*, between 1R and 0.5R, up to 0.5D distance, the flow is characterized by a velocity deficit of 90%: this is due the pressure gap generated by the blade, responsible of the aerodynamic force. Into the *zone 3*, the presence of the hole increases the flow velocity up to 3.5 m/s (Venturi effect). In this area the velocity deficit is negative. After 5D, the central hole has deployed its double effect: the first one accounts the pressure drop, or suction effect, by countering the wake expansion and keeping a "cylindrical like" shape. The second effect is the velocity deficit quick containment, confining the residual turbulent area within 6D, almost concentrated around the Z-axis. It is also noticeable that *zone 1* is getting wider, as depicted in Figure 7, which reports the previous results, and draws the wake morphology.

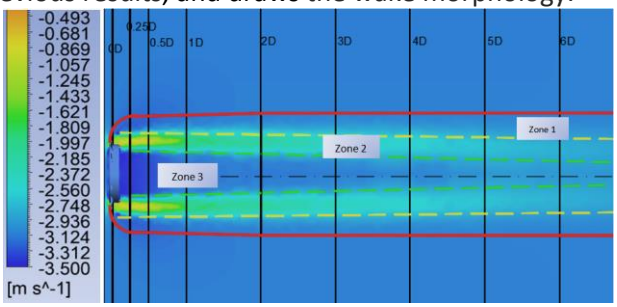


*Figure 7: Wake morphology deployment (not to scale)*

## 4. DISCUSSION

### *4.1 Jensen model for the open centre geometry*

It is possible to apply the Jensen model at the current turbine, by revising the eq. (2) on the base of the CFD output.

To better understand the *a* and *a'* meaning, in Figure 8 the velocities triangle is depicted:

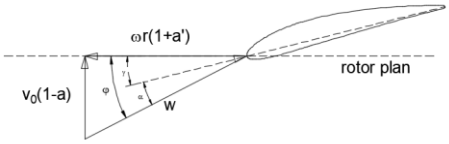


*Figure 8: velocities triangle at an inflow blade section*

*w* is the relative velocity, *α* is the attack angle, *φ* inflow angle, and *γ* the pitching angle, $\omega_0 r(1+a')$ is the tangential velocity. *a* is the axial induction factor, reducing $v_0$ due to the presence of the rotor: it represents a loss of kinetic energy. *a'* is named tangential induction factor and, similarly to *a*, represents the loss of the rotational energy induced by the rotor onto the wake. The equations, relating *a* and *a'*, from Figure 8 are:

$$tan\varphi = \frac{(1-a)v_0}{(1-a')\omega_0 R} \qquad (6)$$

In the eq. (2), the axial velocities are known along the Z and Y axes, the unknown is $C_T$ which can be expressed as:

$$C_T = 4a(1-a) \qquad (7)$$

where *a* also is unknown. To calculate $C_T$, two further equations must be introduced.

The eq. (8) expresses *T* (turbine Thrust), known from CFD (see Table 2), as function of the water density *ρ*, the flow velocity $v_0$, and rotor swept area $A_0$, known from design (see Table 1):

$$T = 2\rho F v_0^2 A_0 a(1-a) \qquad (8)$$

With the eq.(9), the tip loss factor *F* [25] is expressed as:

$$F = \frac{2}{\pi}\arccos\left[e^{-\left(\frac{b}{2}\frac{R-r}{r\sin\varphi}\right)}\right] \quad (9)$$

where $\varphi$ is done by the design, $b$ is the number of blades, and $R - r$ the difference between the turbine external radius and the central hole one (see Table 1). By combining the eq. (7), (8), and (9), it results that $a$ = 0.26 and $C_T$ = 0.76. Once calculate $a$, eq.(6) yields $a'$ = 0.04.

In Figure 9, the blue curve is obtained from the Jensen equation (2) rearranged with the CFD output as above calculated ($a$, $a'$, $C_T$). The red curve represents the axial velocity deficit data from CFD, expressed as root square mean including the values in the XY plane.

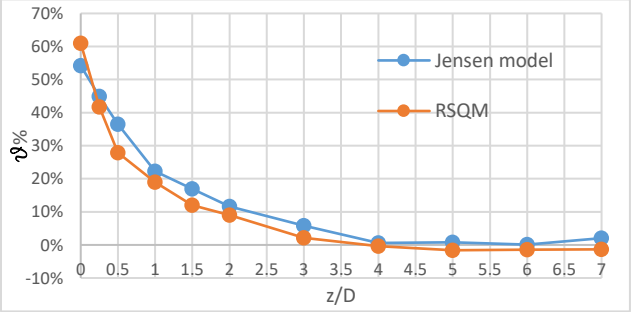


*Figure 9: axial velocities deficit curves*

### 4.2 Wake characteristics

The wake angular velocity $\omega_w$ is:

$$\omega_w = 2a'\omega_0 \quad (10)$$

The $\omega_w$, as calculated with the previous data equals 1.04 rad/s. This value highlights the slow wake rotation, 7.7% of the rotor one. This velocity is estimated at a very close distance (about 0.1D) from the rotor and demonstrates the low energized wake. For comparison [262] the traditional turbines account a higher value of the tangential induction factor $a'$. A lower wake expansion is also due to a limited torque $M$. From the Momentum theory, suitable to evaluate the main turbine performances, by introducing the wake rotation, $M$ can be calculated as:

$$dM = 2a'(1-a)\rho v_0\omega_0 r^2(2\pi r dr) \quad (11)$$

The integral of eq. (11) is calculated considering the external radius $R$ and the central hole one $r_i$. Since $M$ depends on the swept area $A_0$ (in this case an annulus), the reduced flow rate passing through the rotor affects any fluid dynamic forces which are proportionally reduced. However, the low wake angular velocity positively affects the wake deployment by reducing the tangential velocity component. As consequence, the wake energy is reduced.

Combining the previous results and the CFD evidence between 0D and 2D, it can be stated that the effects of the blades' rotation affect the early flow field, due to the tangential and radial components combination (the mentioned tangential induction factor $a'$, see eq.(6)). In this zone, the suction effect counters the centrifugal components, limiting the wake enlargement (as CFD evidenced, up to 1.6R). The wake rotation it is about 7% the rotor angular velocity.

According to the CFD results, the fluid domain can be decomposed into 2 subdomains, *Sd1* (0D ~2D) and *Sd2* (2D ~6D).

1. In *Sd1* the maximum velocity deficit is achieved for $y_{max}$ =1.6R then the velocity deficit modifies the trend. From eq. (1) the wake aperture can be calculated as (with $y_{ref}$ = R):

$$k = \frac{y_{max} - y_{ref}}{\Delta D} \quad (12)$$

   where $\Delta D$ =2D=4R. In these conditions *k(0-2D)* = 0.16.
2. For *Sd2*, since $y_{ref}$=$y_{max}$ the wake shape is cylindrical.

### 4.3 2 device layout

To apply the previous results, this section investigates an initial array arrangement, composed by 2 turbines in different patterns, accommodated by varying two parameters: the wheelbase *w*, the distance between the turbines' rotational axes, and *m*, the distance between turbines' rotational planes, even known as distance between rows.

Due to early stage of the study, a domain diameter of 9D has been adopted, with a blockage ratio $b_r$ = 0.04 (4%). Each turbine is modelled with the sliding mesh.

Under the previous assumptions, a second CFD simulations' batch has been carried out. The output parameters to be considered are the array power coefficient $C_{pa}$, and the power $P_1$ and $P_2$ respectively exploited by each turbine. The suitability of the configuration is based on the single rotor performance: the power loss of each rotor should lower than 10% of the stand-alone one.

Two basic turbine layouts have been investigated as depicted in Figure 10, respectively named *Case 0* and *Case 1* so to fix the performances of a double devices pattern.

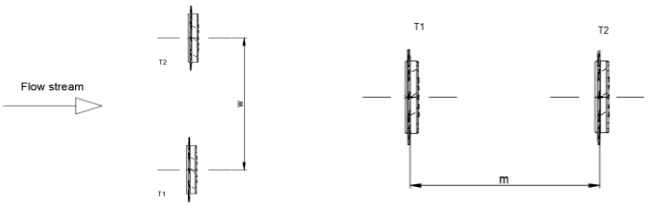


*Figure 10: Case 0 (left) and Case 1 (right) (not to scale)*

Table 3 reports the performances: for the *Case 0*, the exploited power is equal for both turbines: they can be considered decoupled.

*Table 3: Case 0 and Case 1, performance*

| Id | Nr device | $C_{pa}$ [-] | $P_1$ [W] | $P_2$ [W] | m [-] | w [-] |
|---|---|---|---|---|---|---|
| *Case 0* | 2 | 0.411 | 1443.85 | 1444.69 | - | 3D |
| *Case 1* | 2 | 0.389 | 1441.88 | 1298.17 | 6D | - |

In *Case 1*, the T1 wake affects T2 and its power is reduced of about 10% because the T2 is still immersed in the T1 downwash. Although the single turbine wake can be analytically considered negligible after 6D, the T1 mixed Zone 2-3 still affects T2.

### *4.4 Double turbines: staggered layout*

In Figure 11, a staggered layout ($w > 0$) has been investigated, to evaluate the benefits.

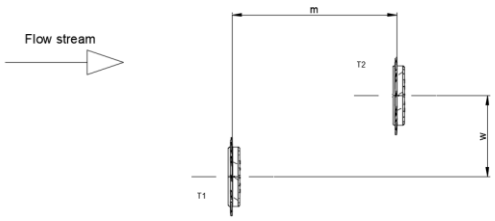


*Figure 11: staggered configuration (not to scale)*

As highlighted in Table 4 the significant result is that $P_1 \approx P_2$. The staggered layout implies that T2 operates outside the main turbulence zone (*zone 3*) induced by T1. T2 takes advantage from such a Venturi effect, increasing the velocity close to the rotor, as displayed in Figure 12.

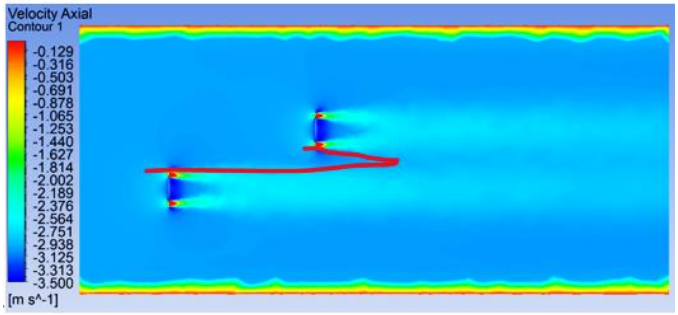


*Figure 12: Venturi effect (the red line bounds the area)*

It is noticeable the wake of both turbines: the red contour highlights that no overlaps occur between the two wakes, indeed, the flow velocity boosts, achieving 3.5 m/s, close to T2 blade tip. To refine the previous results, some further CFD runs have been carried out. The results are reported in Table 4. that the staggered layout consents to install two turbines at $m$=5D and $w$ = 2.5D (*Case 4*) without significant interferences.

*Table 4: 2 turbines layout: performance comparison vs m and w*

| id | Nr devices | $C_{pa}$ [-] | $P_1$ [W] | $P_2$ [W] | m [-] | w [-] |
|---|---|---|---|---|---|---|
| *Case 2* | 2 | 0.412 | 1445.80 | 1450.42 | 6D | 3D |
| *Case 3* | 2 | 0.410 | 1446.40 | 1435.80 | 6D | 2D |
| *Case 4* | 2 | 0.412 | 1445.64 | 1452.20 | 5D | 2.5D |

## 5. CONCLUSIONS

The effects of the main configuration parameters, such as the length and width of the wake phenomena behind an open centre turbine, have been investigated by CFD simulation.

The central hole increases the axial velocity, like a Venturi duct, so reducing the pressure in a cylindrical zone around the Z-axis. The pressure drop counters the flow enlargement in the 0D~2D range, the radial and tangential velocity components slightly prevail enlarging the wake cone and inducing a radial expansion of 1.6R corresponding to a wake aperture k=0.16. After 2D, those components are mitigated by the axial one, keeping constant the wake aperture with a cylindrical shape. The flow velocity, initially overcoming the inflow one, reduces up to 6D. After 2D.

However, the wake morphology plays a fundamental role in the array design. A staggered configuration has been selected as the most performing one, due to the Venturi effect generated by the annular rotor in combination with the external wake of the early devices. The rear device benefits of this effect when its rotor is slightly immersed in the peripheral wake zone of the early turbines.

Compared to the traditional turbines array, the distance between rows results lower (5D vs 7D), despite the wheelbase is kept at 2.5D (vs 3D), resulting to be more compact in an array purpose.

## REFERENCE

[1] Jensen N.O., A note on wind generator interaction. 1983, Risø National Laboratory

[2] Larsen G.C., A simple wake calculation procedure. 1988

[3] Bahaj A.S., Myers L.E., Thomson M.D., Jorge N. Characterising the wake of horizontal axis marine current

turbines. In: Proceedings of the 7th European Wave and Tidal Energy Conference 2007
[4] Chen Y., Lin B., Lin J., Wang S., "Experimental study of wake structure behind a horizontal axis tidal stream turbine," Appl. Energy, vol. 196, pp. 82–96, 2017.
[5] Zhang Y., Zhang J., Zheng Y., Yang C., Zang W., Fernandez-Rodriguez E., "Experimental analysis and evaluation of the numerical prediction of wake characteristics of tidal stream turbine," Energies, vol. 10, no. 12, p. 2057, Dec. 2017
[6] Stansby P., Stallard T. "Fast optimisation of tidal stream turbine positions for power generation in small arrays with low blockage based on superposition of self-similar far-wake velocity deficit profiles," Renew. Energy, vol. 92, pp. 366–375, 2016
[7] Ahmadi M.H.B. "Influence of upstream turbulence on the wake characteristics of a tidal stream turbine," Renew. Energy, vol. 132, pp. 989–997, 2019
[8] Badoe C.E., Edmunds M., Williams A.J., Nambiar A., Sellar B., Kiprakis A., Masters I. Robust validation of a generalised actuator disk CFD model for tidal turbine analysis using the FloWave ocean energy research facility, Renewable Energy, Volume 190, 2022, Pages 232-250, ISSN 0960-1481, https://doi.org/10.1016/j.renene.2022.03.109.
[9] Barbarelli S., Amelio M., Castiglione T., Florio G., Scornaienchi N.M., Cutrupi A., Lo Zupone G., Analysis Of The Equilibrium Conditions Of A Double Rotor Turbine Prototype Designed For The Exploitation Of The Tidal Currents. Proceedings of "SDEWES 2013", Dubrovnik, Croazia, 22-27 September 2013
[10] Lo Zupone G., Amelio M., Barbarelli S., Florio G., Scornaienchi N.M., Cutrupi A. LCOE evaluation for a tidal kinetic self-balancing turbine: Case study and comparison, Applied Energy doi:10.1016/j.apenergy.2016.01.015, Pages 1292-1302
[11] Barbarelli S., Florio G., Lo Zupone G., Scornaienchi N.M., First technical evaluation of array configuration of self-balancing tidal kinetic turbines, Renewable Energy, Renewable Energy 129 (2018) 183e200
[12] Lo Zupone G., Barbarelli, S, Liu, C, Yan, J, Liang, B. Open center tidal turbine: How a new mooring system concept affects the performances. Int J Energy Res. 2020; 1– 18. https://doi.org/10.1002/er.6266
[13] Lo, Zupone Giacomo Francesco and Fiore, Enrico and Barbarelli, Silvio and Castiglione, Teresa. Kinetic modular machine for producing energy from fluid flows. US Patent 17047321. Jan 04, 2022
[14] Ott S., Berg J., Nielsen M. Linearised CFD models for wakes, Technical Report Risø–R–1772(EN), Risø National Laboratory for Sustainable Energy, Roskilde, 2011
[15] Batten W.M.J., Bahaj A.S., Molland A.F., Chaplin J.R. Hydrodynamics of marine current turbines. Renew Energy 2006;31(2):249e56
[16] Peña A., Réthoré P.E., van der Laan M.P. (2016) On the application of the Jensen wake model using a turbulence-dependent wake decay coefficient: the Sexbierum case. Wind Energ., 19: 763– 776. doi: 10.1002/we.1863
[17] Liu J., Htet L., Srinivasa R.P., Wake field studies of tidal current turbines with different numerical methods, Ocean Engineering, Volume 117, 2016, Pages 383-397, ISSN 0029-8018, https://doi.org/10.1016/j.oceaneng.2016.03.061
[18] Myers L., Bahaj A.S. Near wake properties of horizontal axis marine current turbines, Proceedings of the 8th European Wave and Tidal Energy Conference, Uppsala, Sweden, 2009
[19] Lee J.H., Park S., Kim D.H., Rhee S.H., Kim M.C. Computational methods for performance analysis of horizontal axis tidal stream turbines. Applied Energy, 2012; 98:512–23. https://doi.org/10.1016/j.apenergy.2012.04.018
[20] Martin O., Hansen L. Aerodynamics of Wind Turbines, Routledge, 2015, ISBN: 978-1-315-76998-1
[21] Nguyen V.T., Guillou S.S., Thiébot J., Santa Cruz A. Modelling turbulence with an Actuator Disk representing a tidal turbine, Renewable Energy, Volume 97, 2016, Pages 625-635, ISSN 0960-1481, https://doi.org/10.1016/j.renene.2016.06.014.
[22] Ahmadi M.H.B., "Influence of upstream turbulence on the wake characteristics of a tidal stream turbine," Renew. Energy, vol. 132, pp. 989–997, 2019
[23] Mycek P., Gaurier B., Germain G., Pinon G., Rivoalen E. Experimental study of the turbulence intensity effects on marine current turbines behaviour. Part I: One single turbine, Renewable Energy 66 (2014) 729-746. doi:10.1016/j.renene.2013.12.036.
[24] ANSYS-Fluent-Tutorial-Guide R17.0, (2016), ANSYS Inc.
[25] Zhong W., Shen W.Z., Wang T., Li Y. A tip loss correction model for wind turbine aerodynamic performance prediction, Renewable Energy, Volume 147, Part 1, 2020, Pages 223-238, ISSN 0960-1481, https://doi.org/10.1016/j.renene.2019.08.125.
[26] Clary V., Oudart T., Larroudé P., Sommeria J., Maître T., An optimally-controlled RANS Actuator force model for efficient computations of tidal turbine arrays, Ocean Engineering, Volume 212, 2020, 107677, ISSN 0029-8018, https://doi.org/10.1016/j.oceaneng.2020.107677.